FERMILAB-Pub-02/352-A January 2003

Clusters and Superclusters in the Sloan Digital Sky Survey

J. Einasto[1], G. Hütsi[1], M. Einasto[1], E. Saar[1], D. L. Tucker[2], V. Müller[3], P. Heinämäki[1,4], S. S. Allam[5,2]

[1] Tartu Observatory, EE-61602 Tõravere, Estonia
[2] Fermi National Accelerator Laboratory, MS 127, PO Box 500, Batavia, IL 60510, USA
[3] Astrophysical Institute Potsdam, An der Sternwarte 16, D-14482 Potsdam, Germany
[4] Tuorla Observatory, Väisäläntie 20, Piikkiö, Finland
[5] National Research Institute for Astronomy & Geophysics, Helwan Observatory, Cairo, Egypt

Received 09.12.2002 / Accepted ...

Abstract. We apply the 2-dimensional high-resolution density field of galaxies of the Early Data Release of the Sloan Digital Sky Survey with a smoothing lengths 0.8 h^{-1} Mpc to extract clusters and groups of galaxies, and a low-resolution field with smoothing lengths 10 h^{-1} Mpc to extract superclusters of galaxies. We investigate properties of density field clusters and superclusters and compare properties of these clusters and superclusters with Abell clusters, and superclusters found on the basis of Abell clusters. We found that clusters in high-density environment have a luminosity a factor of $\sim$ 5 higher than in low-density environment. There exists a large anisotropy between the SDSS Northern and Southern sample in the properties of clusters and superclusters: most luminous clusters and superclusters in the Northern sample are a factor of 2 more luminous than the respective systems in the Southern sample.

Key words. cosmology: observations – cosmology: large-scale structure of the Universe; clusters of galaxies

arXiv:astro-ph/0212312 v1 13 Dec 2002

1. Introduction

Clusters and groups of galaxies are the basic building blocks of the Universe on cosmological scales. The first catalogues of clusters of galaxies (Abell 1958, Zwicky et al. 1961–68) were constructed by visual inspection of the Palomar Observatory Sky Survey plates. More recent catalogues of clusters, as well as catalogues of groups of galaxies, have been derived using catalogues of galaxies (Huchra, Davis, Latham, & Tonry (1983), Dalton et al. (1997)). Moving up the hierarchy of large-scale structure, galaxy cluster catalogues themselves have been used to define still larger systems such as superclusters of galaxies (Einasto et al. 1994, 1997, 2001, hereafter E94, E97 and E01).

The goal of the present paper is to map the Universe up to redshift $z = 0.2$ and to find galaxy clusters and superclusters using the density field method. The application of the density field is not new. In the pioneering study by Davis & Huchra (1982) the density field was used to calculate the gravitational field of the nearby Universe. Gott, Melott & Dickinson (1986) used the density field to investigate topological properties of the Universe. Bertschinger et al. (1990) calculated the potential, velocity, and density fields from redshift-distance data. Saunders et al. (1991) applied the density field to map the Universe, to find superclusters and voids, and calculated moments of the density field. Marinoni et al. (1999) reconstructed real space local density field. In these studies nearby optical or infrared galaxy samples were used. More recently, Hoyle et al. (2002) used smoothed 2-dimensional density fields from volume limited subsamples of SDSS EDR galaxies to discuss the 2-dimensional geometry of the large-scale matter distribution in comparison with ΛCDM simulations, and Sheth et al. (2002) advertised a new method of evaluating isodensity contours of smoothed 3-dimensional density fields from simulations for characterizing topological properties of the supercluster-void network.

We calculate the density field of the Sloan Digital Sky Survey Early Data Release (SDSS EDR) by Stoughton et al. (2002), as described by Hütsi et al. (2002, hereafter Paper I), to find clusters and superclusters of galaxies, and to investigate their properties. Clusters of galaxies from the SDSS were extracted previously by Goto et al. (2002) using the cut and enhance method; Kim et al. (2002) compared various cluster detection algorithms based on SDSS data. In this paper we define clusters as enhancements of the density field and use various smoothing lengths to separate systems of galaxies of different size and luminosity. We use a high-resolution density field to find clusters and groups of galaxies. For simplicity, we use the term "DF-clusters" for both groups and clusters found

Send offprint requests to: J. Einasto

Table 1. Data on SDSS EDR galaxies, clusters and superclusters

Sample	DEC	RA	ΔRA	α_1	M_1^*	α_2	M_2^*	$N_{\rm gal}$	$N_{\rm cl}$	$N_{\rm ACO}$	$N_{\rm scl}$
SDSS.N	0°	190.25°	90.5°	−1.06	−21.55	−1.22	−20.80	15209	2868	22	24
SDSS.S	0°	23.25°	65.5°	−1.06	−21.40	−1.10	−20.71	11882	2287	16	16

in the high-resolution density field of galaxies. Similarly, we use a low-resolution density field to construct a catalogue of superclusters of galaxies, and denote them as "DF-superclusters". DF-clusters and superclusters are defined as enhancements of the density field, DF-clusters in a fixed volume ($\pm 2.5\ h^{-1}$ Mpc from the centre), and DF-superclusters as high-density regions surrounded by a fixed isodensity contour. In determining DF-clusters and superclusters we take into account known selection effects. We shall investigate some properties of DF-clusters and superclusters, and study these clusters and superclusters as tracers of the structure of the local Universe.

This study is of exploratory character to find the potential of SDSS data to analyse the structure of the Universe both on small and large scales. In this stage we use the fact that SDSS EDR covers only relatively thin slices; thus we calculate the density field in 2 dimensions only. As more data will be made available we plan to use a full 3-dimensional data set to detect clusters and superclusters of galaxies. In this exploratory stage of the study we will make no attempt to convert distances of galaxies and systems of galaxies from redshift space to true space. This correction applies only to positions of galaxies and clusters, not to their luminosity. Due to smoothing of the density field, small-scale corrections (e.g., the "Finger-of-God" Effect) are practically flattened out.

Although there are large-scale corrections due to the apparent contraction of superclusters in redshift space (the Kaiser Effect, Kaiser 1984), the actual positional shifts of supercluster centres are very small; furthermore, they do not alter cluster and galaxy positions in tangential direction. The only large-scale redshift distortion is the radial contraction of superclusters, not the number and luminosity of clusters within superclusters. Since supercluster shapes are not the main target of this present study, we may ignore this effect for now.

In Section 2 we give an overview of the observational data. In Section 3 we find DF-clusters and investigate their properties. Similarly, in Section 4 we compose a catalogue of DF-superclusters, identify them with conventional superclusters, and study their properties. In Section 5 we continue the study of DF-clusters and superclusters, derive the luminosity function of DF-clusters, and analyse these systems as tracers of the large-scale structure of the universe. Section 6 brings our conclusions. The three-dimensional distribution of DF-clusters and superclusters in comparison with Abell clusters and superclusters is shown on the web-site of Tartu Observatory. The analysis of the density field of LCRS shall be published by Einasto et al. (2003).

2. Observational data

2.1. SDSS Early Data Release

The SDSS Early Data Release consists of two slices of about 2.5 degrees thickness and 65 − 90 degrees width, centred on celestial equator, one in the Northern and the other in the Southern Galactic hemisphere (Stoughton et al. 2002). This data set contains over 30,000 galaxies with measured redshifts. We obtained from the SDSS Catalogue Archive Server angular positions, Petrosian magnitudes, and other available data for all EDR galaxies. From this general sample we extracted the Northern and Southern slice samples using following criteria: redshift interval $1000 \le cz \le 60000$ km s^{-1}, Petrosian r^*-magnitude interval $13.0 \le r^* \le 17.7$, right ascension and declination interval $140° \le RA \le 240.0°$ and $-1.2° \le DEC \le 1.2°$ for the Northern slice, and $340° \le RA \le 60.0°$ and $-1.25° \le DEC \le 1.25°$ for the Southern slice. The number of galaxies extracted and the mean RA and DEC are given in Table 1. Distances to galaxies and their absolute magnitudes were calculated as described in Paper I. In calculating the distances we used a cosmological model with a matter density of $\Omega_{\rm m} = 0.3$ and a dark energy density (cosmological constant) of $\Omega_\Lambda = 0.7$ (both in units of the critical cosmological density). Throughout this paper, the Hubble Constant is expressed as usual in units of $H_0 = h\ 100$ km s^{-1} Mpc^{-1}. In calculating absolute magnitudes we used K-corrections and correction for absorption in the Milky Way (for details see Paper I).

2.2. Abell clusters and superclusters

We shall use the sample of rich clusters of galaxies by Abell (1958) and Abell et al. (1989) (hereafter Abell clusters), compiled by Andernach & Tago (1998), with redshifts up to $z = 0.13$. The sample contains 1665 clusters, 1071 of which have measured redshifts for at least two galaxies. This sample was described in detail by E01, where an updated supercluster catalogue of Abell clusters was presented. Superclusters were identified using a friend-of-friends algorithm with a neighbourhood radius of 24 h^{-1} Mpc.

Fig. 1. Absolute magnitudes of galaxies (black dots), and magnitudes of the luminosity window, M_1 and M_2 (coloured dots aligned in almost straight lines), for the Northern slice.

3. Density field clusters

We shall apply the density field to find density enhancements – DF-clusters. The procedure consists of several steps: (1) determining the parameters of the luminosity function needed in the calculating the weights of galaxies, (2) smoothing of the density field, and (3) finding clusters (density enhancements) in the field. Our method of cluster finding assumes that clusters lie completely within the slice, and that there are no other clusters with identical $x, y-$coordinates but shifted vertically. These assumptions are fulfilled in most cases. The extraction of clusters in SDSS survey using full 3-dimensional density field information is planned in the future.

In calculating the density field we make two assumptions. First, we regard every galaxy as a visible member of a density enhancement (group or cluster) within the visible range of absolute magnitudes, M_1 and M_2, corresponding at the distance of the galaxy to the observational window of apparent magnitudes. This assumption is based on observations of nearby galaxies, which indicate that there are really almost no isolated galaxies except perhaps very low-luminosity and diffuse galaxies not represented in surveys like the SDSS. Most galaxies belong to poor groups like our own Galaxy, where one bright galaxy is surrounded by a number of faint satellites. Further, we assume that the luminosity function derived for a representative volume can be applied also for individual groups and galaxies. As we shall see later, this last assumption is not correct, and we must use various galaxy luminosity functions in order to calculate density fields suitable for finding DF-clusters and DF-superclusters. The parameters of the luminosity function (Schechter 1976), α and M^*, are given in Table 1.

We are interested to find total luminosities of DF-clusters and superclusters, thus we shall use in the following analysis the luminosity density rather than the number density. Under these assumptions the estimated total luminosity per one visible galaxy is

$$L_{tot} = L_{obs} W_L, \tag{1}$$

where $L_{obs} = L_\odot 10^{0.4\times(M_\odot - M)}$ is the luminosity of the visible galaxy of absolute magnitude M, and

$$W_L = \frac{\int_0^\infty L\phi(L)dL}{\int_{L_1}^{L_2} L\phi(L)dL} \tag{2}$$

is the weight (the ratio of expected total luminosity to expected luminosity in the visibility window). In the last equation $L_i = L_\odot 10^{0.4\times(M_\odot - M_i)}$ are luminosities of the observational window corresponding to absolute magnitudes of the window M_i, and $M_\odot$ is the absolute magnitude of the Sun. This procedure was used by Tucker et al. (2000) in the calculation of total luminosities of groups of galaxies.

As an example, we plot in Figure 1 for the Northern slice the absolute magnitudes of the window, M_1 and M_2, as well as observed absolute magnitudes of galaxies, M_{obs}. In upper panels of Figure 2 we show luminosity density weights W_L for both sets of the luminosity function. For comparison we show also number-density weights W_N, calculated as described in Paper I. Lower panels of Figure 2 show luminosities of galaxies L_{obs}, and expected total luminosities L_{tot} calculated with eq. (1). Luminosities are expressed in units of 10^{10} Solar luminosities. We see that the number-density weight W_N rises monotonically with increasing distance from the observer, whereas the luminosity density weight W_L rises also toward very small distances. This is due to the influence of bright galaxies outside the observational window, which are not numerous (see the weight W_N) but are very luminous. On larger distances the weight W_L rises again due to the influence of faint galaxies outside the observational window. In calculation of the relative density field only densities in units of the mean density matter, and in this respect the mean distance dependence of L_{tot} is not very different from the distance dependence of the number-density $N_{tot} \propto W_N$.

The next step is the smoothing of the field by a Gaussian kernel and detecting of density field clusters. Here the proper choice of the smoothing length plays a crucial role. Tests with various smoothing lengths have shown that with increasing smoothing length we can find systems of galaxies of increasing scale from clusters and groups and galaxy and cluster filaments to superclusters and their aggregates. Figure 3 shows the density field of the Northern slice calculated with dispersions $0.8 - 16\ h^{-1}$ Mpc. To find DF-clusters with properties close to those of conventional clusters and groups a high-resolution density field is to be used with smoothing scale comparable to the characteristic scale of clusters and groups. The harmonic mean radius of groups and clusters in the Las Campanas Redshift Survey lies in the range

Fig. 2. Upper panels show weights as a function of distance. Grey symbols indicate number-density weights, black symbols luminous-density weights. Lower panels plot luminosities of galaxies as a function of distance. Grey circles mark luminosities of observed galaxies, black symbols total luminosities, corrected for unobservable part of the luminosity range, eq. (1). Left panels are for luminosity function parameters of set 1, and right panels for set 2, which yield better DF-clusters and DF-superclusters, respectively.

$0.45 - 0.65\ h^{-1}$ Mpc (Tucker et al. 2000, Einasto et al. 2002). Abell, APM, and X-ray clusters which have been matched to Las Campanas clusters have harmonic mean radii in the same range. We have used a larger smoothing length, $0.8\ h^{-1}$ Mpc, to identify DF-clusters; this smoothing length is equal to the upper quartile of harmonic radii of groups and clusters (Einasto et al. 2002). With this smoothing length and Gaussian density profile we get density distributions which match satisfactorily surface density profiles of clusters of galaxies (Carlberg et al. 1997). Thus we get a reasonable size of groups even in the case when groups are represented by only a single bright galaxy (we repeat that we consider every galaxy as a representative of a group which includes galaxies outside the observational magnitude window). Most massive clusters in our sample are represented by a number of galaxies with a spread in spatial positions. Thus a modest Gaussian widening does not considerably distort the actual profile of the cluster. After the Gaussian smoothing we get density maps shown in Figure 3 – 5.

The final step is the identification of the DF-clusters. To identify DF-clusters of galaxies, every cell of the field was checked to see whether the density of the cell exceeded the density of all neighbouring cells. If the density of the cell was higher than that of all its neighbours, then the cell was considered as the centre of a DF-cluster and its x, y-coordinates, density value, and luminosity were measured. Inspection of the density field has shown that practically all compact systems of galaxies (groups and clusters) contain their luminous mass within a box of size $-2 \leq \Delta x \leq 2$, and $-2 \leq \Delta y \leq 2$ in cell size units. The luminosity was derived by adding luminosity densities of the 24 surrounding cells to the luminosity density of the central cell. All densities and luminosities were calculated in Solar luminosity units. We also calculated the density in units of the mean density, this relative density was used in Figures 3 – 5 for plotting. A cluster was added to the list of DF-clusters if its luminosity $\mathcal{L}$ exceeds a certain threshold value; we used the threshold $\mathcal{L}_0 = 0.4\ 10^{10}\ L_\odot$. This threshold exceeds the luminos-

Fig. 3. Density field of the SDSS EDR Northern slice, smoothed with $\sigma = 0.8\ h^{-1}$ Mpc, 2 h^{-1} Mpc, 10 h^{-1} Mpc, and 16 h^{-1} Mpc dispersion. Upper panels were calculated for parameter set 1 (better reproduction of clusters), lower panels for set 2 (better reproduction of superclusters). In all cases the density field was reduced to a sheet of constant thickness.

ity of poorest groups by a factor of about 2, the number of groups below this limit is very small, see Figure 6. All used cells were marked and in the search for new clusters cells already counted were not included. Figure 4 shows that there are only a few galaxies in the nearby region, $d < 100\ h^{-1}$ Mpc. Moreover, near the outer boundary of the sample, $d > 550\ h^{-1}$ Mpc, samples are already diluted. Therefore, we shall confine our DF-cluster catalogue to the

Fig. 4. Density field of the SDSS EDR slices, smoothed with $\sigma = 0.8\ h^{-1}$ Mpc dispersion.

Fig. 5. Density field of the SDSS EDR slices, smoothed with $\sigma = 10\ h^{-1}$ Mpc dispersion. Open circles note positions of Abell clusters located within boundaries of slices.

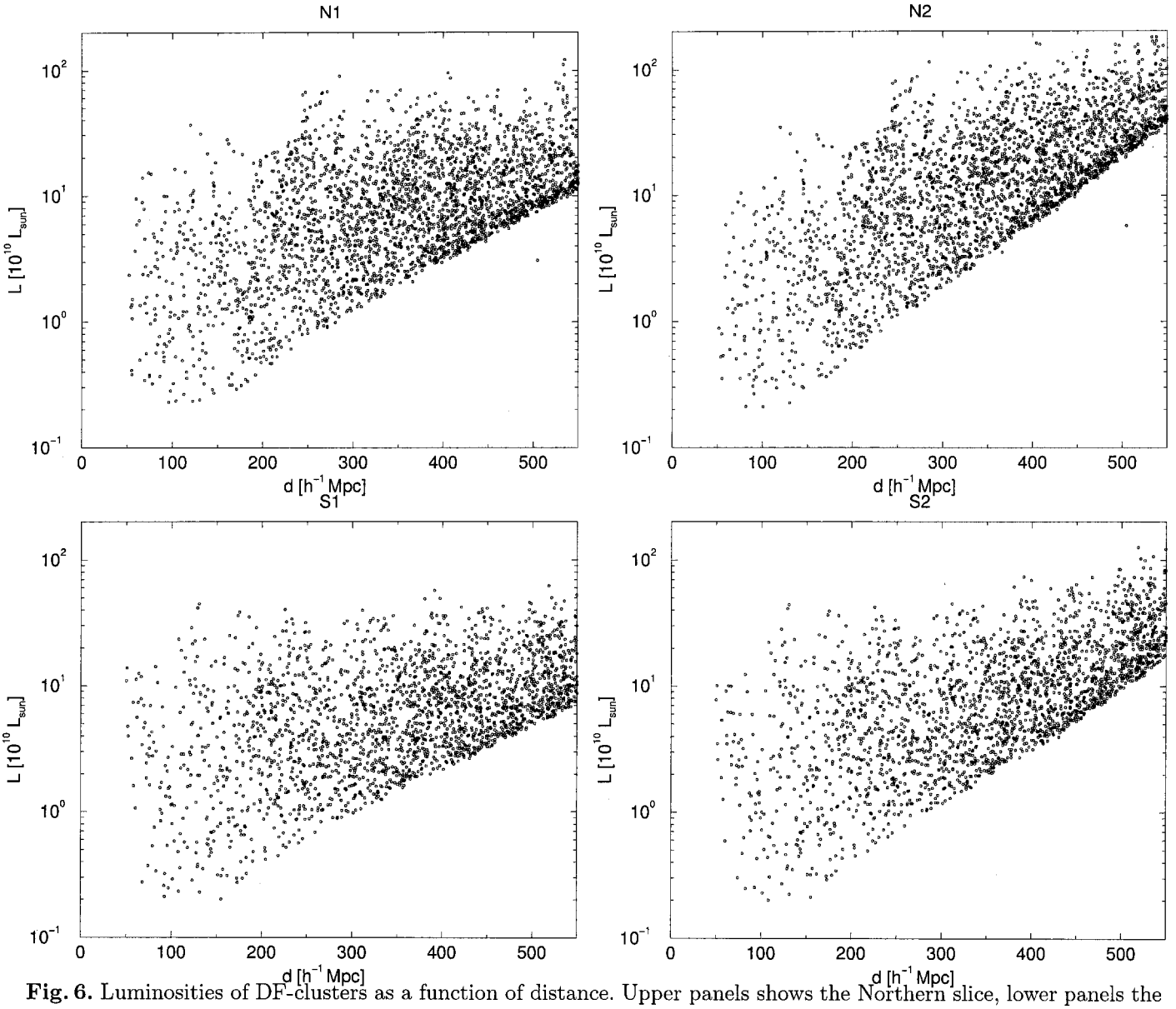

Fig. 6. Luminosities of DF-clusters as a function of distance. Upper panels shows the Northern slice, lower panels the Southern slice; left and right panels represent parameter set 1 and 2, respectively.

distance interval $100 \leq d \leq 550\ h^{-1}$ Mpc. The total number of DF-clusters found is given in Table 1.

Now we look at the properties of DF-clusters. Figure 6 shows luminosities of DF-clusters as a function of distance from the observer, d. The lowest luminosity clusters are seen only at a distance $d \leq 150\ h^{-1}$ Mpc. There exists a well-defined lower limit of cluster luminosities at larger distances, the limit being linear in the $\log L - d$ plot. Such behaviour is expected as at large distances an increasing fraction of clusters does not contain any galaxies bright enough to fall into the observational window of absolute magnitudes, $M_1 \ldots M_2$. The cluster lower luminosity limit is somewhat lower for the Southern slice. The reason for this difference is not yet clear. Nonetheless, the absence of low-luminosity clusters at large distances can be taken into account in calculation of the cluster luminosity function (see section 5 below).

According to general cosmological principle the mean density of luminous matter (smoothed over superclusters and voids) should be the same everywhere. Some weak dependence on distance may be due to evolutionary effects: luminosities of non-interacting galaxies decrease as stars age; but luminosities of merging galaxies (central galaxies of clusters) increase with age. Both effects are rather small within the redshift range $z \leq 0.2$ used in this work (Shepherd et al. (2001)). If we ignore these effects we may expect that the luminous density should not depend on the distance from the observer, in contrast to the number of galaxies which is strongly affected by selection effects (at large distances we do not see low-luminosity galaxies). This difference between the observed and total luminosity is well seen in Figure 2: with increasing distance the weight W_L (the ratio of the total-to-observed luminosity) increases by a factor of 3 (parameter set 1) or even 15 (parameter set 2). We can use the mean total

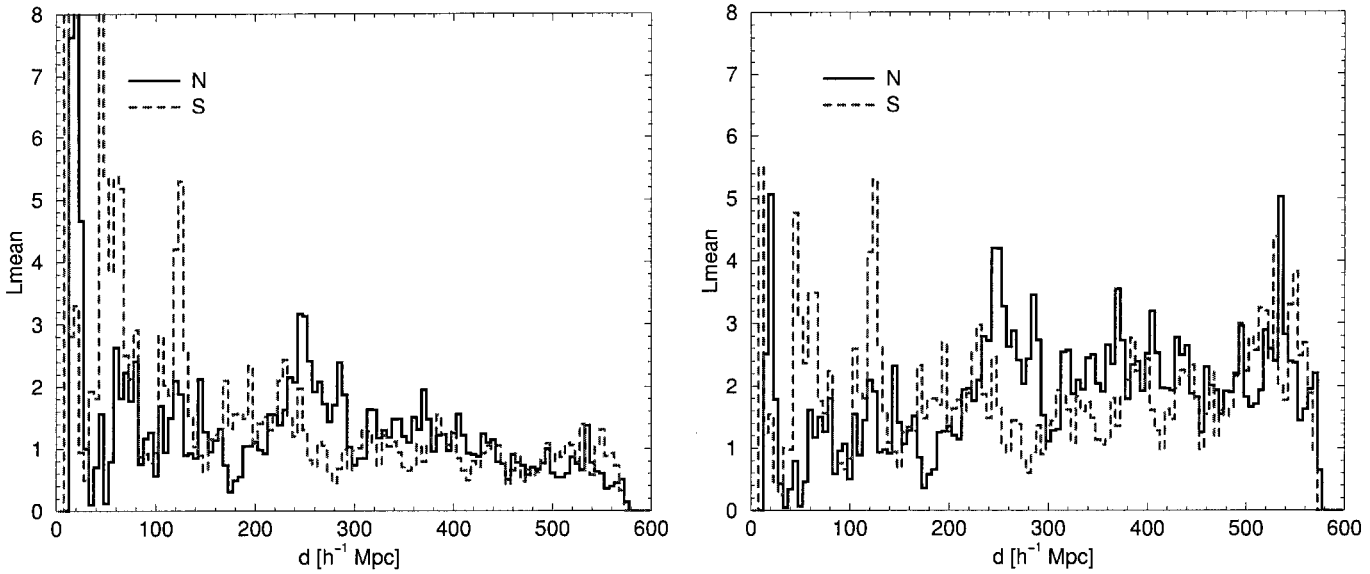

Fig. 7. The luminosity density of SDSS EDR Northern and Southern slices as a function of distance, for luminosity function parameters of set 1 (left) and 2 (right).

luminous density as a test of our weighting procedure. In Figure 7 we show the mean luminous density in spherical shells of thickness 5 h^{-1} Mpc for N and S slices of the SDSS EDR. We see strong fluctuations of the luminous density due to superclusters and voids. The nearby volume is small, so density fluctuations are large at distances $d \leq 220\ h^{-1}$ Mpc; here we also see a low-density region in the Northern slice (see also Figures 3 – 5). At large distances, the overall mean density for parameter set 2 is almost constant. However, in this case the luminosity of clusters rises considerably with distance, and all very massive clusters are concentrated near the outer border of samples (see Figure 6).

In determination of the parameter set 2 the number of faint unobservable galaxies in calculation of the luminosity function was estimated using Schechter parameters for the whole sample. As we have seen above, faint clusters are not visible at large distances. Thus, in order to estimate correctly the total number of faint galaxies, the luminous mass of invisible clusters has been added to visible clusters, and the luminosity of visible clusters has been overestimated. To get correct luminosities of clusters we have used the parameter set 1 which yields more or less uniform level of high-mass clusters at various distances from the observer, see left panels of Figure 6. Schechter parameters of this set correspond to a subsample of galaxies in high-density environment, dominating in more distant regions. Using this set we find, that luminosities of most massive clusters also increase with distance. However, a small increase is expected since the volume of distant shells is larger, and thus the probability to find a bright galaxy in a shell of fixed thickness is higher on larger distance from the observer. Using the luminosity function shown in Paper I we estimate that most luminous clusters near the outer border of the sample should be a factor of about 1.25 times more luminous than clusters in the middle of the sample. Figure 6 shows that this is the case for both the Northern and Southern slice for parameter set 1. For this set of parameters the mean luminous matter density decreases with distance, as seen from Figure 7.

The distributions of the mean density and of the cluster luminous masses are very sensitive tests for parameters of the luminosity function. Our tests show that it is impossible for one set of parameters to satisfy both criteria, the distance independence of the mean luminous density and that of the distribution of luminosities of clusters.

4. Density field superclusters

Superclusters have been traditionally defined either as clusters of clusters of galaxies (Oort 1983, Bahcall 1988), or as enhancements in the galaxy distribution (de Vaucouleurs 1953, Saunders et al. 1991, Basilakos, Plionis, & Rowan-Robinson 2001, Kolokotronis, Basilakos, Plionis 2002). In the first case Abell clusters were used to compile supercluster catalogues (E94, E97, E01). In the second case superclusters were found by using the distribution of individual galaxies or by using smoothed density field maps. Here we follow the density field approach and use the low-resolution density field to find large overdensity regions which we call density field superclusters (or DF-superclusters). Tests with various smoothing lengths showed that a smoothing length $\sigma_{sm} = 10\ h^{-1}$ Mpc yields a catalogue of superclusters with properties similar to those of known superclusters.

The compilation of the supercluster catalogue consists of three steps: (1) calculating the density field, 2) finding overdensity regions, and 3) determining the properties of the resulting superclusters. The density field was calculated as described above with one difference – in order to reduce the wedge-like volume of slices to a sheet of uniform thickness we divided densities by the thickness of the slice

at each particular distance. In this way the surface density of the field is on average independent of distance, and we can use a distance independent search for overdensity regions. The reduced density field for the Northern and Southern SDSS EDR slices is shown in Figure 5.

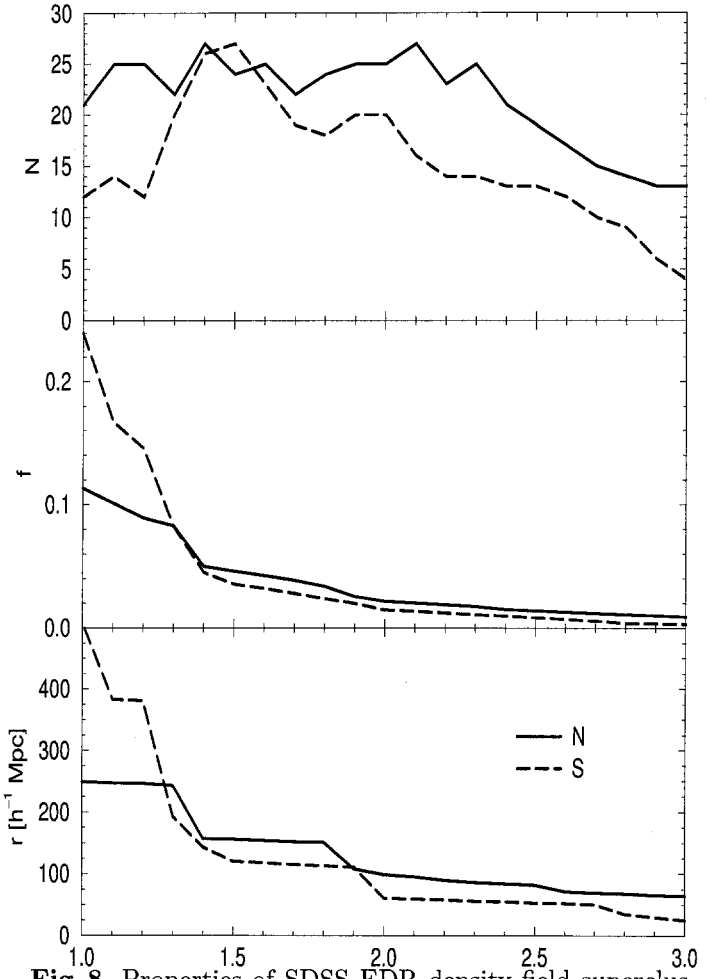

Fig. 8. Properties of SDSS EDR density field superclusters as a function of the threshold density, ϱ_0, to separate superclusters (high-density regions) and voids (low-density regions). The upper panel shows the number of superclusters, N, the middle panel the area of the largest supercluster (in units of the total area of the slice), and the lower panel – the diameter (either in x or y direction, whatever is larger) of the largest supercluster.

Next we searched for connected high-density regions. To do so we need to fix the threshold density, ϱ_0, which divides high- and low-density regions. This threshold density plays the same role as the neighbourhood radius used in the friends-of-friends (FoF) method to find clusters in galaxy samples and to find superclusters in cluster samples. If we have a high threshold density (this corresponds to a small neighbourhood radius), we get as connected regions only the central peaks of superclusters – the number of peaks is small, high-density regions cover only a small area, and their diameters are small. When we decrease the threshold density – corresponding to an increase in the neighbourhood radius in the FoF method – then the number of high-density regions increases and their areas and diameters also increase. When the threshold density is too low, then superclusters merge to form large complexes, their masses and diameters grow, and at a certain threshold density percolation occurs, i.e. the largest supercluster spans across the whole region under study.

To make a proper choice of the threshold density we plot in Figure 8 the number of superclusters, N, the area of the largest supercluster f (in units of the total area of the slice), and the maximum diameter of the largest supercluster (either in the x or y direction) as a function of the threshold density ϱ_0 (we use relative densities here). Data are given for both the Northern and the Southern slices. We see that the number of superclusters for the Northern slice has a broad maximum between $1.3 < \varrho_0 < 2.3$, for the Southern slice the maximum is sharper at $\varrho_0 \sim 1.5$. For lower ϱ_0 large superclusters are merged; for higher ϱ_0 fewer regions are counted as high-density. The area and diameter of the largest supercluster continue to drop rapidly until $\varrho_0 \sim 2.0$. This shows that various criteria suggest different values for the threshold density. We have used a threshold density $\varrho_0 = 1.8$. At this threshold density the largest supercluster still has a diameter over 100 h^{-1} Mpc, it has several concentration centres (local density peaks), and its area forms a large fraction of the total area of the slice. The merging of large superclusters can be followed when we look for sudden changes in the relative area and diameter. For both slices superclusters are separated at $\varrho_0 = 2.1$; this density value is used to resolve the largest supercluster into sub-superclusters. Superclusters were found over the distance interval $100 \leq d \leq 555$ h^{-1} Mpc. We include only superclusters with areas greater than 100 $(h^{-1}\,\mathrm{Mpc})^2$; otherwise we get as superclusters tiny regions with diameters of less than 10 h^{-1} Mpc.

The number of superclusters in each of the two slices is shown in Table 1. In Table 3 we list for individual superclusters positional, physical, and morphological data. To aid in identifying these superclusters, we provide an identification number No, the right ascension RA, the distance d, and rectangular coordinates, x, and y (in h^{-1} Mpc) used in the density field plots. The column labelled "Id" gives indicates the identification number from E01 of any matches to previously known superclusters based upon the Abell cluster sample.

For physical data we present the observed total luminosity of the supercluster L_{obs} (sum of observed luminosities of DF-clusters located within the boundaries of superclusters), the estimated total luminosity of the superclusters L_{tot}, the diameter D of the supercluster (diameter of a circular area equal to the area of the supercluster), and $\Delta = max(dx, dy)$, where dx and dy are diameter of the supercluster in the x and y direction. The difference between the diameter D and Δ yields information on the flattening of the supercluster in the plane of the slice. For round systems $D \sim \Delta$; for elongated superclusters, Δ ex-

ceeds D. The total luminosity L_{tot} was calculated from the observed luminosity L_{obs}

$$L_{tot} = \frac{D}{D_d} L_{obs}, \quad (3)$$

where D_d is the thickness of the slice at the distance of the centre of the supercluster, and we have assumed that the vertical diameter of the supercluster is identical to the diameter in the plane of the slice D. Finally, f is the fraction of the area of the supercluster in units of the total area occupied by superclusters in a given slice.

For morphological data we give the number of DF-clusters and Abell clusters lying within the boundaries of the supercluster, N_{cl} and N_{ACO}, respectively, see also Figure 5. Following is the type of the supercluster "T", estimated by visual inspection of the density field. Here we have used the following tentative classification: if the supercluster shows filamentary character, then its type is "F" for a single filament or "M" for a system of multiple filaments. As an example of a filamentary system we refer to supercluster N04; an example of a multi-filamentary system is the supercluster N02. N04 consists of a single well-defined filament, and N02 of two massive filaments situated at almost right angles to each other. In both cases the main filaments are surrounded by a loose cloud of faint clusters. If such diffuse clusters dominate and the filamentary character is not evident, then the supercluster morphology is listed as a diffuse "D", an example being N08. Finally, "C" denotes a compact supercluster without clear filamentary system, an example being N15. This classification is based on the distribution of galaxies and clusters in a plane. If 3-dimensional data were available, then the true shape of each supercluster could be established.

It should be noted that most superclusters are surrounded by faint systems of galaxies, either in the form of filaments or of a diffuse cloud of clusters. Thus the distinction between a filamentary and diffuse system is not very strict.

5. DF-clusters and superclusters as traces of the structure of the universe

5.1. Selection effects

The main selection effect in the SDSS survey is due to the finite width of the apparent magnitude window, which excludes galaxies brighter or fainter than this window. The presence of a relatively narrow visibility window affects our results in two different ways. First of all, it influences the number and luminosity of galaxies in DF-clusters. This effect can be taken into account statistically in the determination of the luminosity of clusters using weighting of galaxies in DF-clusters. But the visibility window also affects the number of DF-clusters – a faint DF-clusters will not be visible at all at large distances if none of its member galaxies is bright enough to fall within the visibility window. The number of faint DF-clusters can be estimated statistically using the procedure described below in calculating the DF-cluster luminosity function. This procedure, however, cannot restore physical parameters or positions of individual invisible DF-clusters, similar to the first procedure which cannot restore parameters of invisible galaxies.

The weighting of visible galaxies in clusters statistically restores properties of clusters which have at least one galaxy in the visibility window of the survey. The procedure depends crucially on the parameters of the galaxy luminosity function which is used to derive the weights for the visible galaxies. We have used the constancy of the mean density with redshift to check the values for the luminosity function (parameter set 2). Our analysis has shown that the mean properties of superclusters are independent of the distance from the observer, which suggests that the global properties of the low-resolution density field are correct. However, in this case, the luminosities of the DF-clusters are too high at these large distances. The reason for the overcorrection of visible cluster luminosities is simple: visible clusters have to include also luminosities of invisible clusters. It is clear that in this case we get a wrong distribution of cluster luminosities. This is clearly seen in Figure 4 of Paper I, where almost all distant clusters seem reddish (they have very high luminous density), whereas in nearby regions clusters have various colours from red to yellow, green and blue, representing clusters of various luminosity.

To avoid this effect we have used another set of values for the parameters of the galaxy luminosity function (parameter set 1). Now we get cluster luminosities which are, in the mean, independent of the distance from the observer. In this case the mean density of luminous matter decreases with distance, as do the mean luminosities of superclusters. This deficit of low-luminosity clusters can be estimated in the determination of the cluster luminosity function (see next section).

There are two possibilities to correct for the second selection effect in the calculation of the density field. We can add to the density field, calculated on the basis of the *observed* galaxies and corrected for unobserved galaxies associated with them, a smooth background which takes into account unseen galaxies not-associated with observed ones. In the calculation of the low-resolution density field this procedure yields the correct large-scale distribution of luminous matter – if the unseen galaxies are distributed randomly. However, this last assumption needs justification: faint galaxy systems, like bright systems, may be preferentially located within superclusters. On the other hand, this procedure also adds some luminous matter to DF-clusters, since luminous matter is collected into DF-clusters from the whole search box $\pm 2.5\ h^{-1}$ Mpc from the cluster centre. In other words, this correction method distorts DF-cluster properties. As we want to derive statistically correct cluster properties, we must use a high-resolution density field without the background correction. Taking into account these difficulties we have used a different method to find the low-resolution density field, by using for clusters and superclusters various parameters of

the galaxy luminosity function. We plan to return to this problem when more SDSS galaxy data become available.

5.2. Luminosity function of DF-clusters

Now we calculate the integrated luminosity function of DF-clusters, i.e. the number of DF-clusters per unit volume exceeding a luminosity L. Figure 6 shows that only very bright DF-clusters are observable over the whole depth of our samples. These bright clusters form a volume limited subsample of DF-clusters. Fainter clusters are seen in the nearby volume only; the estimated total number of fainter clusters can be found by multiplying the observed number of clusters by a weighting factor of $(d_{lim}/d_L)^3$, where $d_{lim} = 550\ h^{-1}$ Mpc is the limiting distance used in compiling of the DF-cluster sample and d_L is the largest distance where clusters of luminosity L are seen. Figure 6 indicates that there exists an almost linear relation between d_L and $\log L$; this relation was used to calculate the weighting factor for clusters of every luminosity. Results for both SDSS samples are shown in Figure 9.

We see that the luminosity functions span over 3 orders in luminosity and almost 4 orders in spatial density. This shows that the SDSS sample is well suited for determining this function from observations. Presently we have not determined masses of DF-clusters; thus it is not possible for us to transform the luminosity function to mass function of clusters. However, if we assume that the mass-to-luminosity ratio of DF-clusters is constant, then we can have an estimate of the DF-cluster mass function. Our luminosity function is not very different from the real observed mass function of conventional clusters and groups of galaxies (Ramella, Pisani & Geller 1997, Girardi & Giuricin 2000, Heinämäki et al. 2002).

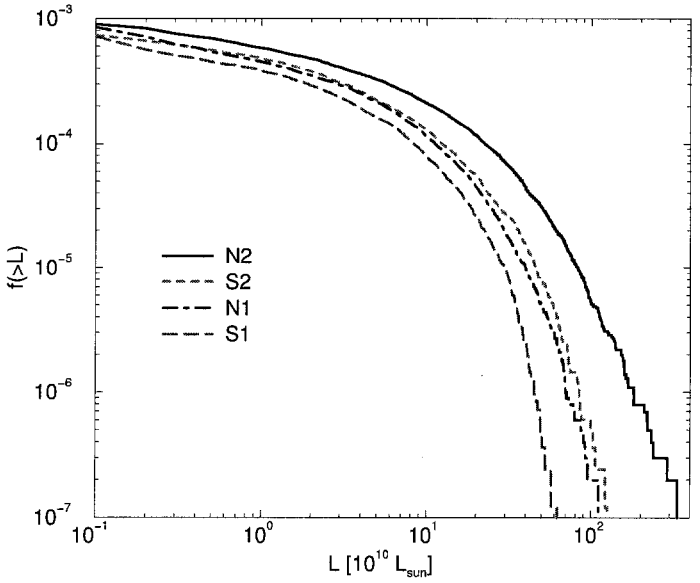

Fig. 9. Integrated luminosity function of DF-clusters for parameter sets 1 and 2.

The integrated luminosity function was found for both parameters sets of the galaxy luminosity function (see Figure 9). The number of bright clusters is much larger for the parameter set 2. As discussed above, this is due to the overcorrection of cluster luminosities – particularly at large distances – to compensate for non-detected faint clusters. Thus we believe that the function for parameter set 1 corresponds better to reality.

Our results also show that the Northern SDSS sample has a larger number of luminous DF-clusters than does the Southern sample. This difference is seen for both parameter sets of the galaxy luminosity function. In order to find the reason for this difference we repeated our calculations using different values for the parameters of the galaxy luminosity function for the Northern and Southern samples, as suggested by the analysis presented in Paper I. This did not change the main result – there exists a considerable difference in the distribution of luminosities of DF-clusters in the Northern and Southern samples. We return to this problem below.

5.3. Environmental effects in the distribution of DF-clusters

We can use the density found with the 10 h^{-1} Mpc smoothing as an environmental parameter to describe the global density in the supercluster environment of clusters. We calculated this global density ϱ_0 (in units of the mean density of the low-resolution density field) for all DF-clusters. Figure 10 shows the luminosity of DF-clusters as a function of the global density ϱ_0. There is a clear correlation between the luminosity of DF-clusters and their environmental density. Luminous clusters are predominantly located in high-density regions, and low-luminosity clusters in low-density regions. This tendency is seen also visually in Figure 4. Here densities are colour-coded, we see that small clusters in voids have blue colour which indicates medium and small densities, whereas rich cluster having red colour populate dominantly central high-density regions of superclusters.

Figure 10 shows also that the Northern sample has much more luminous clusters than the Southern sample. This result confirms the presence of a difference between the structure of Northern and Southern samples.

Figure 11 shows the cluster luminosity functions of the Northern and Southern slice calculated separately for 4 global density intervals, $0 < \varrho_0 \leq 0.5$, $0.5 < \varrho_0 \leq 1.0$, $1.0 < \varrho_0 \leq 1.8$, and $1.8 < \varrho_0 \leq 10$, labelled in Figure and Table 2 as N0.0, N0.5, N1.0 and N1.8, for Northern subsamples, and S0.0, S0.5, S1.0, S1.8 for Southern ones. The functions were calculated for the luminosity function parameter set 1 (which yields almost constant highest luminosity DF-clusters for various distances from the observer). We list in Table the number of DF-clusters in subsamples, $N_{\rm group}$, the luminosity of most-luminous clusters, $L_{\rm lum}$, the mean luminosity of clusters, L_m, and the scatter of luminosities, σL_m. We see that luminosity func-

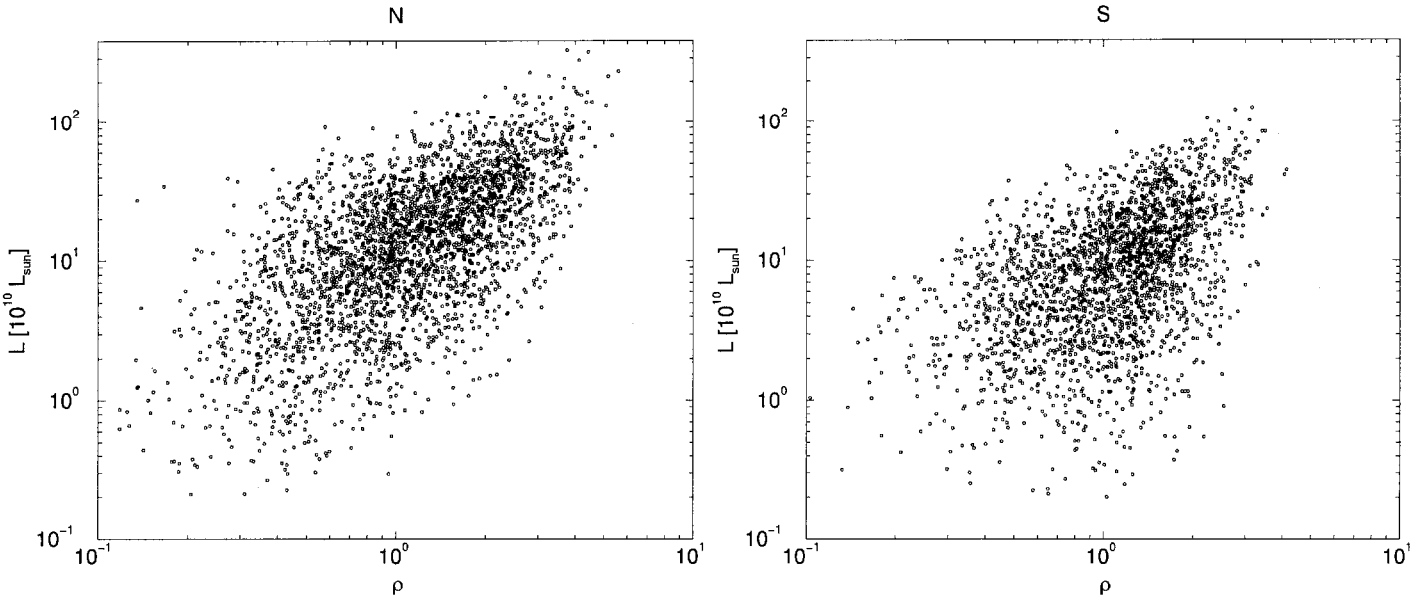

Fig. 10. Luminosities of DF-clusters as a function of the global relative density ϱ_0. Left panel shows the Northern slice, right panel the Southern slice.

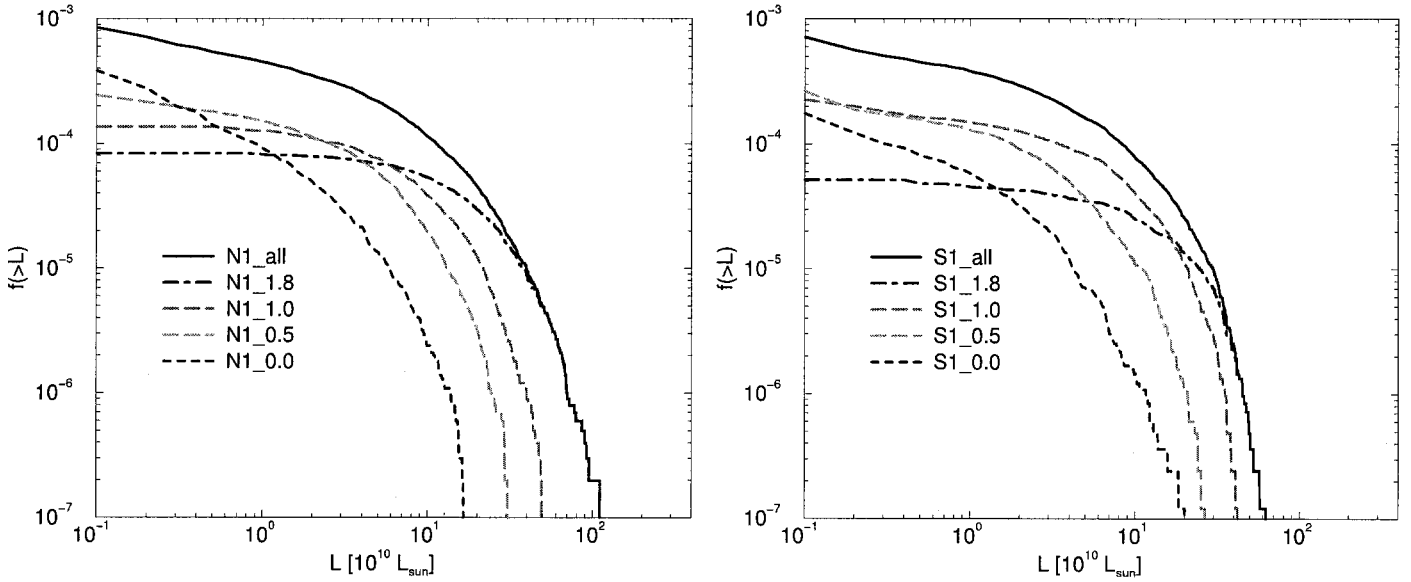

Fig. 11. Integrated luminosity functions of DF-clusters as a function of the global relative density ϱ_0. Left panel shows the Northern slice, right panel the Southern slice.

tions depend very strongly on the global environment: the difference in luminosity of most luminous clusters in subsamples is a factor of 5 ± 2. This difference is not due to different numbers of clusters, as these numbers are all of the same order.

One may ask: How much of the cluster luminosity–environment relation be explained by the fact that a luminous cluster itself contributes to the luminosity density of the supercluster? At an extreme, suppose there is only one cluster in the supercluster. In that case, the supercluster's luminosity density is determined entirely by the single cluster. In reality, small scatter of the luminosity–environment relation at high environmental density is probably due just to proximity to luminous clusters themselves. This influence decreases when we move toward lower environmental densities. We plan to investigate this problem, as well as the influence of selection effects to the luminosity-density relationship of DF-clusters when more SDSS data will be available. The influence of selection is minimal to luminosities of most-luminous clusters.

Fig. 12. A view to Abell clusters in equatorial coordinates. Filled circles show Abell clusters located in superclusters of richness 8 and more members, open circles mark Abell clusters in less rich superclusters. Strips near the celestial equator note SDSS slices, the Northern slice is in the left side. Area surrounded by coloured lines indicates regions where rich superclusters of the Dominant Supercluster Plane are located. Large filled circles near the equator in the middle of the Northern slice show clusters of supercluster SCL 126. The Galactic zone of avoidance has in equatorial coordinates a S-shaped curve.

Table 2. Luminosities of DF-clusters

Sample	$N_{\rm group}$	$L_{\rm lum}$ $10^{10}L_{sun}$	L_m $10^{10}L_{sun}$	σL_m $10^{10}L_{sun}$
N0.0	438	17.9	3.66	2.52
N0.5	852	33.5	7.20	4.09
N1.0	872	50.7	11.30	6.28
N1.8	716	121.5	21.72	12.35
S0.0	277	20.0	3.57	2.15
S0.5	695	26.5	5.60	3.30
S1.0	965	42.1	9.57	5.48
S1.8	341	62.3	16.93	9.84

5.4. The fine structure of superclusters and voids

The distribution of DF-clusters within DF-superclusters yields information on the internal structure of superclusters. A close inspection of Figures 4 and 5 shows, that superclusters have various internal structures: clusters may form a single filament, a branching system of filaments, or a more or less diffuse cloud of clusters. These morphological properties have been characterised by types F, M, D, and C in Table 3. This Table shows that almost all massive superclusters have morphological type M, i.e. they are multi-branching. Faint superclusters do not have a dominant morphological type: among faint superclusters we find all morphological types.

In the Northern sample about 25 % of all DF-clusters are located in superclusters; in the Southern sample this fraction is about 15 %. An inspection of the high-resolution density map in Figure 4 shows that most DF-clusters outside superclusters also form filaments. Thus we come to the conclusion that there is no major difference in the shape of cluster systems in supercluster and in non-supercluster environments. This similarity of the structure within and outside superclusters is partly due to our formal procedure of defining superclusters; actually there is a continuous sequence of structures from single filaments to multiple filaments and superclusters. The difference is mainly in the luminosity of clusters. This observation can be interpreted as follows: clusters and cluster filaments in various environments are formed by similar density perturbations, and these small-scale perturbations are modulated by large-scale perturbations which make clusters and their filaments richer in superclusters and poorer in large voids between superclusters [see also Frisch et al. (1995)].

Figure 13 shows the distribution of total luminosities of DF-superclusters at various distances from the observer. We see that both high and low luminosity superclusters are found both in nearby space as well as in more distant regions. This distribution is expected for real superclusters, and we may expect that there are no serious systematic errors in the luminosities of DF-superclusters.

Table 3 shows that there are only a few dozen Abell clusters in EDR SDSS sheets. In comparison with DF-clusters Abell clusters form a small minority of clusters, and their distribution does not match the distribution of even luminous DF-clusters, see Figure 5 (we note that

in some cases mismatch of Abell and DF-clusters may be due to distance errors of Abell clusters). Thus it is evident that, simply from number statistics alone, Abell clusters are not as good a structure indicator as are DF-clusters.

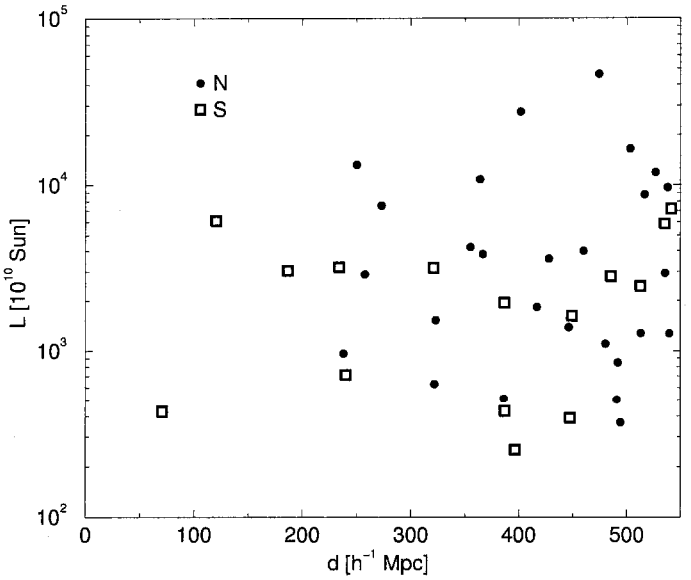

Fig. 13. Total luminosities of DF-superclusters in SDSS EDR slices at different distances from the observer.

5.5. DF-superclusters in the supercluster-void network

Now we analyse DF-superclusters as tracers of the large-scale supercluster-void network. First we note that most nearby DF-superclusters can be identified with the Abell supercluster catalogue of E01, which contains superclusters out to a distance limit of 350 h^{-1} Mpc (see Table 3 and Figure 5). Now we comment on some individual superclusters.

The supercluster N13 (SCL 126 in the list by E01) has the densest concentration of Abell and X-ray clusters in our neighbourhood. The densest part of this supercluster has a declination $-2.5°$ and lies in the $-3°$ slice of the Las Campanas Redshift Survey. It contains 7 Abell clusters and 6 X-ray clusters, most of which are located within the LCRS slice. Both in the SDSS and LCRS slices the supercluster shows a multi-branching filamentary shape. The form of the filaments in both slices is different. This is a good indication that cluster chains form true filaments, not sheets, since at the distance of the supercluster both slices are vertically shifted by only about 12 h^{-1} Mpc.

Another very rich supercluster is N08 (Virgo-Coma; SCL 111 in E01's list). This supercluster contains 15 Abell clusters and 5 X-ray clusters. Its centre lies at declination $+9°$; thus the SDSS slice passes through the outskirts of this supercluster. Not far from E01 SCL 111 lies the supercluster SCL 91 in the list by E97 (Leo-Sextans); it contains 9 Abell clusters and 1 X-ray cluster at declination $+3°$. This supercluster is seen as a density enhancement in Figure 5; its density in the SDSS slice is, however, too low to include this feature as a supercluster in the present catalogue.

There are two more very rich superclusters in the Northern slice: SCL 107 from E97 (N07) with 8 Abell clusters and 1 X-ray cluster, and SCL 100 from E97 with 9 Abell clusters. Their centres lie at declinations $+10°$ and $-3°$, respectively, and they form together with supercluster SCL 111 (N09) a huge complex near the centre of the SDSS Northern slice. These superclusters, and superclusters SCL 82 and SCL 91 belong to the Dominant Supergalactic Plane – a collection of very rich superclusters in the nearby Universe (E97).

The richest supercluster in the Southern slice, according to Abell supercluster catalogue, is the Pegasus-Pisces SCL 3 from E97 (or S01 in our catalogue) with 9 Abell clusters, 6 X-ray clusters, and a centre at declination $+5°$. The second richest supercluster in the Southern slice is the Pisces SCL 24 (S10) with 7 Abell clusters and 10 X-ray clusters and a centre at declination $+8°$. The SDSS Southern slice passes through the periphery of these superclusters.

5.6. The North–South asymmetry in the distribution of clusters and superclusters

One of principal results of our study is the discovery of a large difference between the distribution of galaxies and clusters in the Northern and Southern slice of the SDSS. A moderate difference is observed in the galaxy luminosity functions, a much larger difference exists between distributions of cluster luminosities and between cluster luminosity functions (see Figure 9, 10, and 11). The North-South asymmetry is seen also as a systematic difference of total luminosities of Northern and Southern DF-superclusters: the Northern sample contains more massive superclusters than the Southern one (see Table 3 and Figure 13). These results indicate the presence of global differences between the Northern and Southern slices.

One possibility to explain these differences in the distribution of clusters and superclusters is by various parameters of the galaxy luminosity function. To check this possibility we varied parameters of the luminosity function of galaxies in accordance with results obtained in Paper I. In all variants tested so far the North-South asymmetry remains. Thus the difference lies probably elsewhere.

Another explanation would be to assume that these differences can be caused by cosmic variance. To check this possibility we compared properties of various systems of galaxies in the Northern and Southern slices. This has lead us to conclude that the most likely explanation of the North-South asymmetry is the presence of real differences in the richnesses of systems of galaxies of various scales. As we have discussed in the previous section, the Northern slice lies in a region of space containing many rich superclusters. The $\pm 10°$ zone around the celestial equator in the right ascension interval of the Northern slice contains

25 Abell superclusters in the catalogue by E01 (15 in the $\pm 6°$ zone). Among these, there are 5 very rich superclusters containing 7 or more Abell clusters (all in the central $\pm 6°$ zone). The $\pm 10°$ zone around the Southern slice has 12 Abell superclusters; the $\pm 6°$ zone has 7 Abell superclusters, among which there is only one very rich system. The distribution of Abell clusters on the celestial sphere is presented in Figure 12. Regions of the SDSS EDR are marked by solid strips, dashed lines show regions where rich superclusters belonging to the Dominant Supergalactic Plane (DSP) are projected on the sky. The DSP was detected by E97. In this plane are concentrated numerous very rich superclusters. We see that the Northern SDSS EDR slice crosses the DSP. Near the supercluster SCL 126 (or N13 in our list) the DSP crosses another region of rich superclusters seen in the Northern hemisphere extending from a declination of $+60°$ to a declination of $-30°$. So the Northern slice lies at crossroads of two complexes of very rich superclusters. In contrast, the Southern slice is located in a region away from very rich superclusters: in the Southern Hemisphere, rich superclusters, some of which belong to the DSP, are located at lower declinations.

Thus our tentative conclusion is that the North-South asymmetry is not a mere random fluke but a real difference in the large-scale distribution of matter. So far this difference is manifested in only a single pair of slices. This result must be checked by future SDSS data.

5.7. Error analysis

There are three main error sources in our quantitative data: errors due to number statistics (Poisson errors), errors in the values for the parameters of the galaxy luminosity function, and errors in our assumptions concerning the constancy of the mean luminous density and the upper end of luminosities of DF-clusters. Our quantitative analysis is related directly to luminosities of DF-clusters. Thus we must analyse how these errors affect cluster luminosities.

The simplest errors are related to the Poisson statistics. In Paper I we determined Poisson errors for parameters of the luminosity function of galaxies. It is easy to estimate the influence of these errors to properties of density field clusters. We have repeated the density field analysis with many sets of parameters. We show here results for a third set of parameters $M^\star = -20.73$ and $\alpha = -1.14$, the difference between sets 2 and 3 being $\Delta M^\star = 0.07$, and $\Delta\alpha = 0.08$, which corresponds approximately to the 2σ error of parameters in the luminosity function (see Paper I). We have found DF-clusters for both parameter sets and made cross-identification of clusters. Cluster positions are practically identical, only total luminosities differ. Both luminosities are compared in Figure 14. We see that there exists a very close relationship with small scatter between luminosities of DF-clusters found with parameter sets 2 and 3. Our main quantitative results (North-South asymmetry of luminosities and dependence of luminosities on environment) are differential, thus errors of parameters of the luminosity function of galaxies do not alter these conclusions.

Fig. 14. Comparison of luminosities of DF-clusters for different parameter sets. In vertical axis we plot luminosities of clusters for parameter set 2, in horizontal axis either for set 1 or 3.

A much more serious systematic difference is due to our poor understanding of the global behaviour of the mean luminosity density, i.e. the third error mentioned above. The influence of this error is also demonstrated in Figure 14, where we compare luminosities of DF-clusters for parameter sets 1 and 2. Here the scatter is much larger – almost all clusters are much brighter for the parameter set 2. This is the reason why cluster luminosity functions for parameter sets 1 and 2 differ so much. The physical reason for this large uncertainty is our poor understanding of the general behaviour of the density field – how constant it should be for different distances from the observer. We plan to come back to this problem in a future study.

There are other sources of uncertainty, ones which influence positions of DF-clusters and superclusters. These errors are due to the fact that in this paper we have used positions of galaxies in redshift space. Redshift space distortions are of two different types: they elongate clusters of galaxies in the radial direction (finger-of-god effect), and they shift positions of DF-clusters and superclusters in the radial direction toward the contraction centre (bulk motions). As superclusters are more massive attractors than clusters, their positions are much less influenced than are positions of clusters. Due to bulk motions supercluster shapes are slightly compressed in the radial direction. The shift is small and does not influence luminosities of clusters and superclusters.

The largest uncertainty in the properties of superclusters is due to the fact that we presently have information only for thin slices. In their largest dimension, a supercluster may extend for hundreds of Mpc; this is much, much larger than the smallest dimension of our slices, their thickness. Therefore, it is impossible to say for certain just what fraction of a given supercluster lies within a slice's boundaries. Our estimate of the total luminosity of superclusters is based on the assumption that they have in vertical direction a structure similar to the structure on the plane observed. This assumption is correct if the observed plane passes close to the centre of the supercluster. If the observed plane passes through the periphery of the supercluster, we get an underestimated value of the total luminosity and diameter. Thus values shown in Table 3 can be considered as lower limits of actual values of the respective quantities.

One possible error of cluster luminosities is due to possible overlapping of clusters in x, $y-$coordinates due to our 2-dimensional detection scheme. The probability of this error is, however, rather low. In the future we plan to define clusters using full 3-dimensional data where this error is excluded.

6. Discussion and conclusions

Results of this paper and Paper I are of a methodical and quantitative character. Methodical aspects concern the application of the density field method with various smoothing lengths to display and describe systems of galaxies of various scales. We calculated density field for a number of smoothing lengths from 0.8 to 16 h^{-1} Mpc. In this way systems of galaxies on various scales could be visualised and their mutual relationship could be studied. The high-resolution density field, with dispersion 0.8 h^{-1} Mpc was used to define density field clusters and to investigate the structure of superclusters. The low-resolution density field, with dispersion 10 h^{-1} Mpc was used to define superclusters of galaxies and to study global properties of clusters and superclusters.

The inspection of the distribution of clusters in superclusters and voids suggests that galaxy systems have in both regions similar shape in that the dominant structural elements are single or multi-branching filaments. Massive superclusters have dominantly a multi-branching morphology; less massive superclusters have various morphologies, including compact, filamentary, multi-branching, and diffuse systems.

Quantitative results concern the luminosity function of galaxies and properties of clusters and superclusters. We have found in Paper I and confirmed in this paper that it is impossible to find a global set of parameters of the luminosity function which can be applied in all cases. We found that parameters of the luminosity function are different for high- and low-density regions: galaxies in high-density regions are more luminous. This result confirms earlier findings by Lindner et al. (1995): bright galaxies define larger voids than faint ones. More recently this conclusion was obtained by Bromley et al. (1998), Beisbart & Kerscher, (2000), and by Norberg et al. (2001). The present study indicates that the effect is larger than previously suspected: luminosities of the brightest galaxies in high-density regions exceed the luminosities of the brightest galaxies in low-density regions by a factor of about 5.

The values of the parameters of the luminosity function are also different for nearby and distant parts of the survey and for the Northern and Southern slices. A distance dependence of parameters of the luminosity function has been found for deeper surveys spanning redshift interval up to $z = 1$ by Lin et al. (1999) and by Shepherd et al. (2001) in the Canadian Network for Observational Cosmology Redshift Survey. However, in this survey the distance dependence appears only by comparison of nearby ($z \sim 0$) and distant ($z > 0.2$) parts of the survey. Thus it seems improbable that this effect can explain our results on the distance dependence in a relatively small redshift interval $0 < z \leq 0.2$.

Parameters of the luminosity function depend also on the density of the environment. This dependence influences properties of the density field. High-density regions contain brighter galaxies than do low-density ones. This difference leads to different selection effects for galaxies in high- and low-density environments. In a high-density environment, due to selection effects, faint galaxies in clusters cannot be observed, but clusters themselves are visible (since they contain at least one galaxy bright enough) and the total luminosity of clusters can be estimated to take into account unobserved galaxies. In a low-density environment all galaxies of the cluster may be too faint, and the cluster may not be seen at all. In another words, distance-dependent selection effects influence clusters and superclusters in different ways.

The density field was calculated using the expected total luminosities of clusters of galaxies, including the expected luminosities of galaxies too faint or too bright to be included in the redshift survey. The correction for unobserved galaxies was made assuming a Schechter luminosity function for galaxies. Our analysis shows that it is impossible to correct the density field so that general properties of the density field and properties of clusters of galaxies are correct for the same set of parameters of the galaxy luminosity function. For this reason we have used two sets of parameters of the luminosity function. Parameter set 1 has a strong bright-end (parameter $M^\star = -21.55$) and corresponds to galaxies in a high-density environment which dominate clusters observed at large distance; this set yields correct properties of clusters of galaxies, but does not include faint clusters at large distances, and thus gives too low of a density for distant superclusters. Parameter set 2 was obtained for the whole region under study, and it has moderate bright-end (parameter $M^\star = -20.80$). In this parameter set ALL faint invisible galaxies at large distance are included within visible clusters, including galaxies that belong to non-detected

clusters; thus clusters themselves become too luminous with increasing distance, but supercluster properties are correct.

Comparing clusters in different environments we have found that there exists a strong dependence of cluster properties on the density of the large-scale environment: clusters located in high-density environments are a factor of 5 ± 2 more luminous than clusters in low-density environments.

Finally we found that there exists a large difference between properties of clusters and superclusters in the Northern and Southern slices of the SDSS EDR survey: clusters and superclusters in the Northern slice are more luminous than those in the Southern slice by a factor of 2. This difference may be due to differences in the location of slices with respect to the very large-scale environment. If this conclusion is confirmed by future observations one must conclude that the formation and evolution of galaxies and systems of galaxies of various scales depends on the nearby as well as on the large-scale environment. Richer superclusters have more luminous galaxies and clusters. On smaller scales this tendency has been observed as a difference between properties of clusters within superclusters and in voids. Now we see that a similar difference may be observed on much larger scales.

Acknowledgements. The present study was supported by Estonian Science Foundation grants ETF 2625, ETF 3601, and ETF 4695 and TO 0060058S98. P.H. was supported by the Finnish Academy of Sciences. J.E. thanks Fermi-lab and Astrophysikalisches Institut Potsdam for hospitality where part of this study was performed.
Funding for the creation and distribution of the SDSS Archive has been provided by the Alfred P. Sloan Foundation, the Participating Institutions, the National Aeronautics and Space Administration, the National Science Foundation, the U.S. Department of Energy, the Japanese Monbukagakusho, and the Max Planck Society. The SDSS Web site is http://www.sdss.org/.
The SDSS is managed by the Astrophysical Research Consortium (ARC) for the Participating Institutions. The Participating Institutions are The University of Chicago, Fermi-lab, the Institute for Advanced Study, the Japan Participation Group, The Johns Hopkins University, Los Alamos National Laboratory, the Max-Planck-Institute for Astronomy (MPIA), the Max-Planck-Institute for Astrophysics (MPA), New Mexico State University, University of Pittsburgh, Princeton University, the United States Naval Observatory, and the University of Washington.

References

Abell, G., 1958, ApJS, 3, 211
Abell, G., Corwin, H. & Olowin, R., 1989, ApJS, 70, 1
Andernach, H. & Tago, E., 1998, in *Large Scale Structure: Tracks and Traces*, eds. V. Müller, S. Gottlöber, J.P. Mücket & J. Wambsganss, World Scientific, Singapore, p. 147
Bahcall, N., 1988, ARAA, 26, 631
Basilakos, S., Plionis, M., & Rowan-Robinson, M., 2001, MNRAS, 323, 47
Beisbart, C. & Kerscher, M., 2000, ApJ, 545, 6
Bertschinger E., Dekel A., Faber S. M., Dressler A., & Burstein D., 1990, ApJ, 364, 370
Bromley, B. C., Press, W. H., Lin, H. & Kirshner, R. P., ApJ, 505, 25
Carlberg R. G., Yee H. K. C.,& Ellingson E., 1997, ApJ, 478, 462
Davis, M. & Huchra, J. 1982, ApJ, 254, 437
Dalton G. B., Maddox S. J., Sutherland W. J., & Efstathiou G., 1997, MNRAS, 289, 263
de Vaucouleurs, G. 1953, MNRAS, 113, 134
Einasto, J., Einasto, M., Hütsi, G., Saar, E., Tucker, D. L., Jaaniste, J., Müller, V., Heinämäki, P., & Allam, S. S., 2003, A&A, (in preparation)
Einasto M., Einasto J., Müller, V., Heinämäki, P.,& Tucker, D. L., 2002, A&A (accepted), astro-ph/0211590
Einasto M., Einasto J., Tago, E., Dalton, G. & Andernach, H., 1994, MNRAS, 269, 301 (E94)
Einasto, M., Einasto, J., Tago, E., Müller, V. & Andernach, H., 2001, AJ, 122, 2222 (E01)
Einasto, M., Tago, E., Jaaniste, J., Einasto, J. & Andernach, H., 1997, A&A Suppl., 123, 119 (E97)
Frisch, P., Einasto, J., Einasto, M., Freudling, W., Fricke, K. J., Gramann, M., Saar, V. & Toomet, O., 1995, A&A, 296, 611
Girardi, M., & Giuricin, G., 2000, ApJ, 540, 45
Goto T., Okamura S., McKay T. A., et al., 2002, PASJ, 54, 515
Gott, J.R., Melott, A.L. & Dickinson, M. 1986, ApJ, 306, 341
Heinämäki, P., Einasto, J., Einasto, M., Saar, E., Tucker, D. L., & Müller, V., 2002, A&A (accepted), astro-ph/0202325
Hoyle, F., Vogeley, M.S., Gott, J.R. et al. 2002, MNRAS, (submitted), astro-ph/0206146
Huchra, J., Davis, M., Latham, D., & Tonry, J. 1983, ApJS, 52, 89
Hütsi, G., Einasto, J., Tucker, D. L., Saar, E., Einasto, M., Müller, V., Heinämäki, P.,& Allam, S. S., 2002, A&A, (submitted) (Paper I)
Kaiser N., 1984, ApJL, 284, L9
Kim R. S. J., Kepner J. V., Postman M., et al., 2002, AJ, 123, 20
Kolokotronis, V., Basilakos, S., & Plionis, M., 2002, MNRAS, 331, 1020
Lin H., Yee H. K. C., Carlberg R. G., Morris S. L., Sawicki M., Patton D. R., Wirth G.,& Shepherd C. W., 1999, ApJ, 518, 533
Lindner, U., Einasto, J., Einasto, M., Freudling, W., Fricke, K.,& Tago, E., 1995, A&A, 301, 329
Marinoni, C.,Giuricin, G. & Ceriani, L. 1999, Proceedings of the 1st Workshop of the Italian Network "Formation and Evolution of Galaxies", pp. 4
Norberg, P., Baugh, C.M., Hawkins, E. et al., 2001, MNRAS, 328, 64
Oort, J.H., 1983, ARAA, 21, 373
Ramella, M., Pisani, A., & Geller, M.J., 1997, AJ, 113, 483
Saunders, W., Frenk, C., Rowan-Robinson, M., Lawrence, A. & Efstathiou, G., 1991, Nature, 349, 32
Saunders, W., Sutherland, W.J., Maddox, S.J. et al., 2000, MNRAS, 317, 55
Schechter, P., 1976, ApJ, 203, 297
Sheth, J. V., Sahni, V., Shandarin, S. & Sathyaprakash, B.S., 2002, MNRAS, (submitted), astro-ph/0210136

Shepherd C. W., Carlberg R. G., Yee H. K. C., Morris S. L., Lin H., Sawicki M., Hall P. B., & Patton D. R., 2001, ApJ, 560, 72

Stoughton, C., Lupton, R. H., Bernardi, M. et al., 2002, AJ, 123, 485

Tucker, D.L., Oemler, A.Jr., Hashimoto, Y., Shectman, A., Kirshner, R.P., Lin, H., Landy, S.D., Schechter, P.L.,& Allam, S.S., 2000, ApJS, 130, 237

Zeldovich, Ya.B., Einasto, J. & Shandarin, S.F. 1982, Nature, 300, 407

Zwicky, F., Wield, P., Herzog, E., Karpowicz M. & Kowal, C.T. 1961–68, Catalogue of Galaxies and Clusters of Galaxies, 6 volumes. Pasadena, California Inst. Techn.

Table 3. The list of superclusters

No	L_{obs} $[10^{10}\ L_\odot]$	L_{tot} $[10^{10}\ L_\odot]$	D Mpc	Δ Mpc	RA deg	d Mpc	x Mpc	y Mpc	f	N_{cl}	N_{ACO}	Id	T
S01	186.6	714.1	24.0	35.0	1.2	239.7	90.5	222.0	0.0205	11	0	3	M
S02	554.2	1621.4	34.4	42.0	4.8	449.0	143.5	425.5	0.0420	20	0		M
S03	345.6	3040.3	43.0	53.0	8.8	186.5	47.0	180.5	0.0655	30	2	19	M
S04	588.1	3164.9	45.2	63.0	9.2	320.9	79.0	311.0	0.0726	33	3	14	M
S05	283.7	642.6	32.8	36.0	9.7	552.4	131.5	536.5	0.0381	7	0		F
S06	159.7	251.8	16.4	23.0	13.2	396.2	70.0	390.0	0.0095	4	0		F
S07	59.8	121.7	29.6	33.0	15.1	554.8	80.0	549.0	0.0310	2	0		C
S08	851.2	2441.7	38.5	45.0	19.2	512.4	37.5	511.0	0.0526	22	0		M
S09	449.8	3187.9	43.4	59.0	23.9	234.0	-2.0	234.0	0.0670	33	1	34	M
S10	379.0	6103.8	50.8	92.0	28.0	120.4	-9.5	120.0	0.0915	29	1	24	M
S11	204.5	429.3	21.3	25.0	28.9	386.8	-37.0	385.0	0.0161	5	0		M
S12	955.7	2798.4	37.2	56.0	31.5	485.3	-68.0	480.5	0.0492	24	0		M
S13	1496.1	5852.5	54.8	65.0	43.2	535.0	-181.0	503.5	0.1066	35	0		M
S14	283.9	389.6	16.1	17.0	45.9	447.5	-171.0	413.5	0.0092	7	0		M
S15	518.9	1943.0	37.9	44.0	52.1	386.4	-185.5	339.0	0.0510	24	0		M
N01	2340.4	8754.9	50.6	85.0	150.6	516.4	331.5	396.0	0.0547	32	0		M
N02	1027.0	7528.6	52.4	71.0	153.9	273.0	163.0	219.0	0.0587	36	4	82	M
N03	709.3	1271.4	25.3	32.0	158.6	539.3	285.5	457.5	0.0137	11	0		F
N04	875.1	3836.5	42.1	67.0	160.4	366.5	184.0	317.0	0.0379	26	0	252	F
N05	1281.3	2943.2	32.2	36.0	166.9	535.4	214.5	490.5	0.0222	13	0		M
N06	267.4	512.4	19.3	22.0	172.9	385.7	117.0	367.5	0.0080	6	0		C
N07	228.8	628.6	23.1	26.0	178.6	321.5	66.5	314.5	0.0114	9	0	107	F
N08	223.5	963.8	26.9	30.0	180.8	238.0	40.5	234.5	0.0154	11	0	111	D
N09	1833.0	10859.9	56.4	84.0	182.3	363.8	52.5	360.0	0.0681	64	2	265	M
N10	6412.0	46426.6	89.9	151.0	184.0	474.1	54.0	471.0	0.1728	116	0		M
N10A	701.1	1832.6	28.5	34.0	190.1	416.5	3.5	416.5	0.0257	20	0		M
N10B	1288.8	3994.9	37.3	40.0	185.6	459.7	39.5	458.0	0.0441	21	0		M
N10C	3616.2	16608.7	60.5	95.0	181.7	503.0	77.5	497.0	0.1158	54	0		M
N11	306.5	367.4	15.5	16.0	185.8	494.2	41.5	492.5	0.0052	5	0		D
N12	393.5	504.7	16.5	19.0	190.7	490.5	-1.0	490.5	0.0058	7	0		D
N13	1446.1	13240.7	59.9	90.0	198.3	249.8	-33.5	247.5	0.0767	56	1	126	M
N14	2704.0	11938.6	60.9	78.0	198.5	526.5	-72.5	521.5	0.0793	50	0		D
N15	428.0	1533.3	30.3	32.0	200.2	323.0	-54.0	318.5	0.0196	12	0		C
N16	1115.7	3590.8	36.0	40.0	207.3	427.7	-123.5	409.5	0.0278	25	0		D
N17	571.3	1101.2	24.2	25.0	209.9	480.1	-159.0	453.0	0.0126	13	0		D
N18	2532.5	9667.2	53.7	69.0	212.1	537.6	-197.5	500.0	0.0618	34	0		M
N19	443.6	847.8	24.6	28.0	215.3	491.5	-205.5	446.5	0.0129	8	0		C
N20	3738.6	27566.5	77.5	94.0	216.8	401.4	-177.5	360.0	0.1285	102	2		M
N21	656.5	1274.0	26.1	33.0	220.1	512.8	-253.0	446.0	0.0145	10	0		C
N22	536.3	2891.5	36.4	57.0	230.0	257.6	-163.5	199.0	0.0283	16	1	153	M
N23	928.3	4221.6	42.3	52.0	230.4	355.0	-227.5	272.5	0.0382	32	1	155	M
N24	595.3	1387.1	27.2	28.0	233.1	445.9	-301.5	328.5	0.0158	13	0		M
S16	1572.5	7159.3	64.5	113.0	359.1	541.1	223.0	493.0	0.1478	45	0		M

Distance, sizes and coordinates are given in h^{-1} Mpc.